Preparation of MgO with High Surface Area, and Modification of Its Pore Characteristics

Moon Hee Lee and Dong Gon Park*

Department of Chemistry, Sookmyung Women's University, Seoul 140-742, Korea
Received January 3, 2003

Thermal decomposition of hydrated surface layer of $Mg(OH)_2$ at 500 °C in vacuum turned non-porous MgO into porous one with high surface area of around 270 m^2/g. Most of its surface area, 74 %, was from micropores, and rest of it was from mesopores in wedge-shaped slits, exhibiting bimodal size distribution centered around 30 and 90 Å. Rehydration followed by subsequent dehydration at 300 °C in dynamic vacuum further raised the surface area to 340 m^2/g. Fraction of microporous surface area was increased to 93%, and the shape of the mesopores was modified into parallel slits with a specific dimension of 32 Å. Application of Fe_2O_3 over MgO *via* iron complex formation did not alter the pore characteristics of MgO core, except slightly increased pore dimension. Over the course of the modification, Fe_2O_3 stayed on the surface possibly *via* spill-over reaction.

Key Words : Magnesium oxide, Surface area, Porosity, Micropore, Hydration

Introduction

Surfaces of metal oxides play an important role in various reactions occurring in nature or in industrial processes. In order to expand understanding on the oxide surfaces, extensive studies have been carried out for various metal oxides.[1] MgO is one of the most frequently chosen model systems for studies on ionic solids. There are more theoretical studies on the surface of MgO than any other metal oxides. But, many studies have pointed out discrepancy between experimental observations and theoretical predictions.[2-9] It has also been observed that the reactivity of MgO toward adsorbed chemicals varies widely depending on how the sample is prepared. For example, organophosphorous compounds and halogenated carbons decomposed more readily on nanocrystalline MgO than on microcrystalline one, which were prepared by different synthetic methods.[10-12] Such variation was caused by different crystalline facets, mainly (100) and (111), and by surface defects such as corners, edges, steps, and kinks. It was also shown that solid-gas reaction between MgO and CCl_4 became stoichiometric, when a layer of Fe_2O_3 was coated over nanocrystalline MgO.[13-16] 'Spill-over' between MgO core and Fe_2O_3 overlayer was considered to be one of a few reasons for the completeness of the solid-gas reaction, which produced environmentally benign $MgCl_2$. Pore property was also presumed to be a major factor to influence the reaction, but not much study has been carried out on it.

Exposed surface of perfect crystal of MgO had been considered to be mainly (100) facet. But, ready take-up of water from atmosphere hardly keeps the surface intact. Recent study showed that normal surface of MgO is (111)-hydroxyl rather than bare (100).[9] As water is chemisorbed on (100) facet in an ambient condition, the surface reconstructs into (111)-hydroxyl, by gaining stability (calculated to be −90.2 kJ/mol) coming from being hydroxylated. Topologically, the (111)-hydroxyl facet of MgO is closely related to (0001) facet of brucite, $Mg(OH)_2$. Both having three-fold symmetry, the (0001) facet of $Mg(OH)_2$ resembles the exposed (111) surface, and (111)-hydroxyl facet of MgO. Therefore, topotactic transformation from MgO to $Mg(OH)_2$ occurs readily on the surface, generating layers of $Mg(OH)_2$ over the core of MgO.

There are many reports on thermal decomposition of brucite ($Mg(OH)_2$) in various conditions, which produces pseudomorphic highly porous MgO.[17-22] It was shown that thermally prompted decomposition of $Mg(OH)_2$ produced pseudomorphic microplates of MgO. The microplates were consisted of smaller nanocubes (nano-grains) of 2-3 nm big, whose (111) direction of the cube was perpendicular to the surface of the plates.[20] The decomposition was also carried out by high-energy electron beam under vacuum, while the surface restructuring was *in-situ* observed.[23] The decomposition was reported to be thermally prompted.

In this study, surface morphology of MgO was modified by thermally decomposing hydroxylated surface layer of $Mg(OH)_2$ over the MgO under dynamic vacuum, and its pore characteristics were investigated. It is anticipated that the track of the decomposition must be same as that reported for the decomposition of bulk brucite.[17-23] The pore characteristics of modified MgO was dependent on the extent of surface hydroxylation. The case with the least amount of hydroxylation was reported in the previous report by author.[24] The case where the initial hydroxylation was maximized is dealt in this report.

Experimental Section

MgO samples were prepared by similar method as described earlier for obtaining CM-MgO (CoMmercially-prepared MgO),[24] except the extent of hydration. The powder of

*To whom correspondence should be addressed. E-mail: dgpark @sookmyung.ac.kr

commercially obtained MgO (micro-grain MgO) was dispersed in distilled water (20 g powder in 250 mL water), and refluxed for 24 h. The hydrated powder was collected by filtration, and dried at 120 °C in an oven during overnight. A few grams of deeply hydrated powder was charged in a 100 mL Schlenk reaction vessel, and thermally processed (dehydration) as described in the previous reports.[15,16] The MgO sample, which went through a cycle of hydration and dehydration under dynamic vacuum, was designated as CP-MgO, following the convention used in the previous report.[14] Overlayer of Fe_2O_3 was applied over the surface of CP-MgO as described in the previous report,[14,24] and the resulting core/shell type product was designated as [Fe_2O_3]CP-MgO, following the convention used in the previous reports.[14]

Further modification of the surface of those samples was carried out by applying an additional cycle of hydration-dehydration. A fraction of each sample, CP-MgO and [Fe_2O_3]CP-MgO, was transferred into an open container, and its surface was hydrated by keeping it under water-saturated air for several days. Subsequent dehydration was carried out for the hydrated samples by heating them at 300 °C for 10 h under dynamic vacuum, converting $Mg(OH)_2$ into MgO.

Powder X-ray diffraction (PXRD) patterns were obtained from powder samples with Philips XPERT MPD diffractometer. FTIR spectra were taken from KBr pellet by using Nicolet Impact-400. Pore property was characterized by measuring nitrogen adsorption-desorption by using ASPS-2400 Micromeritics. Exposure of the samples to humidity was minimized during the analysis. BET surface area and pore size distribution were obtained from the nitrogen adsorption-desorption isotherms.[25] Information on micropores in the samples was analyzed by t-plots derived from the isotherms.[25,26]

Results and Discussion

The isotherm for the adsorption-desorption of nitrogen on the surface of CP-MgO is shown in Figure 1a. Overall shape of the hysteresis corresponds to H3-type for slit-shaped mesopores.[25] But, skewed deviation from ideal shape shows that the isotherm is combination of two segments of the hysteresis. Pore size distribution was calculated by BJH method from nitrogen desorption curve,[27] and is shown in Figure 1c. It is obvious that the size of the mesopores is bimodal, centered around 30 and 90 Å. It appears that slits took wedge-like position, rather than to be parallel, generating two different domains in the size of the mesopores. Distributions around those centers are fairly broad, especially in CP-MgO before modification.

By seeing the distribution trailed off into the pores less than 10 Å, major fraction of total pores is considered to be micropores, rather than meso- or macropores. In order to get information on the micropores, t-plots were calculated from the isotherms and shown in Figure 3. The fitted line intercepts at high volume, which indicates large portion of

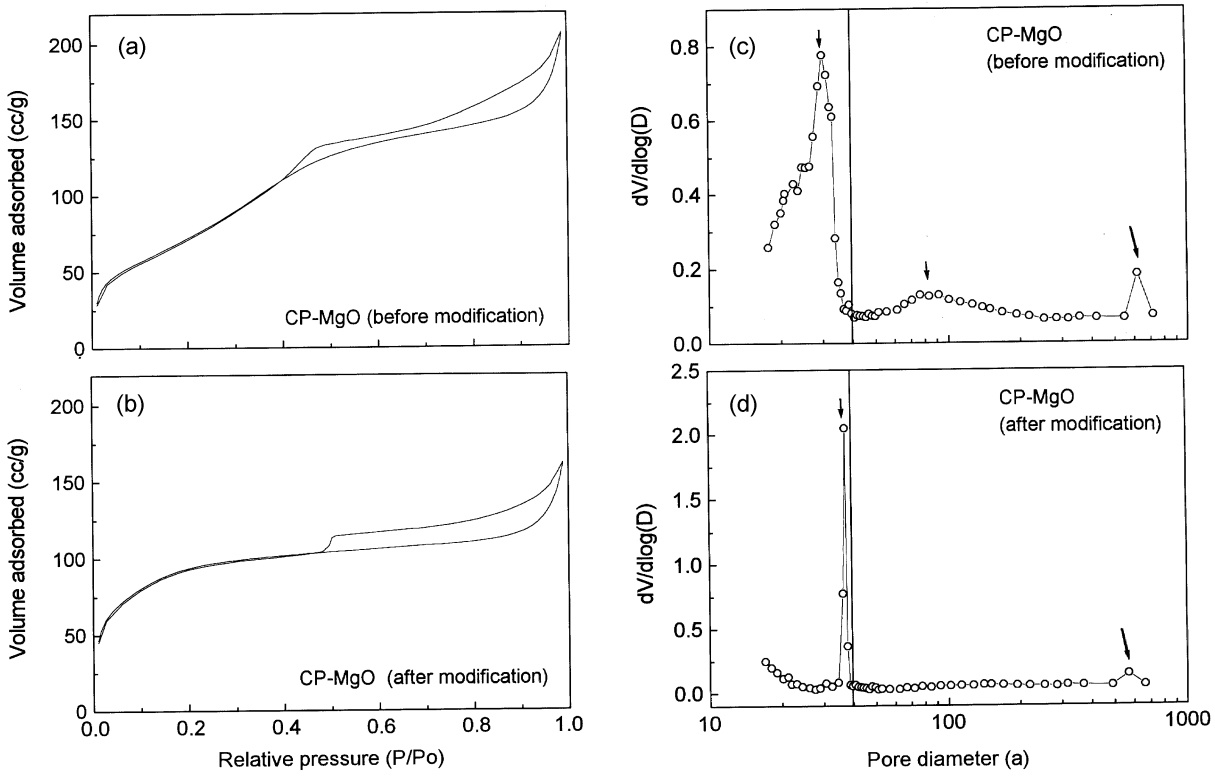

Figure 1. Isotherms of nitrogen adsorption-desorption on the surface of CP-MgO. (a) before modification, and (b) after modification. Pore size distributions of CP-MgO, derived from desorption curves in the isotherms. (c) before modification, and (d) after modification. Pore characteristics of CP-MgO was modified by hydration in water-saturated air, followed by dehydration at 300 °C under dynamic vacuum.

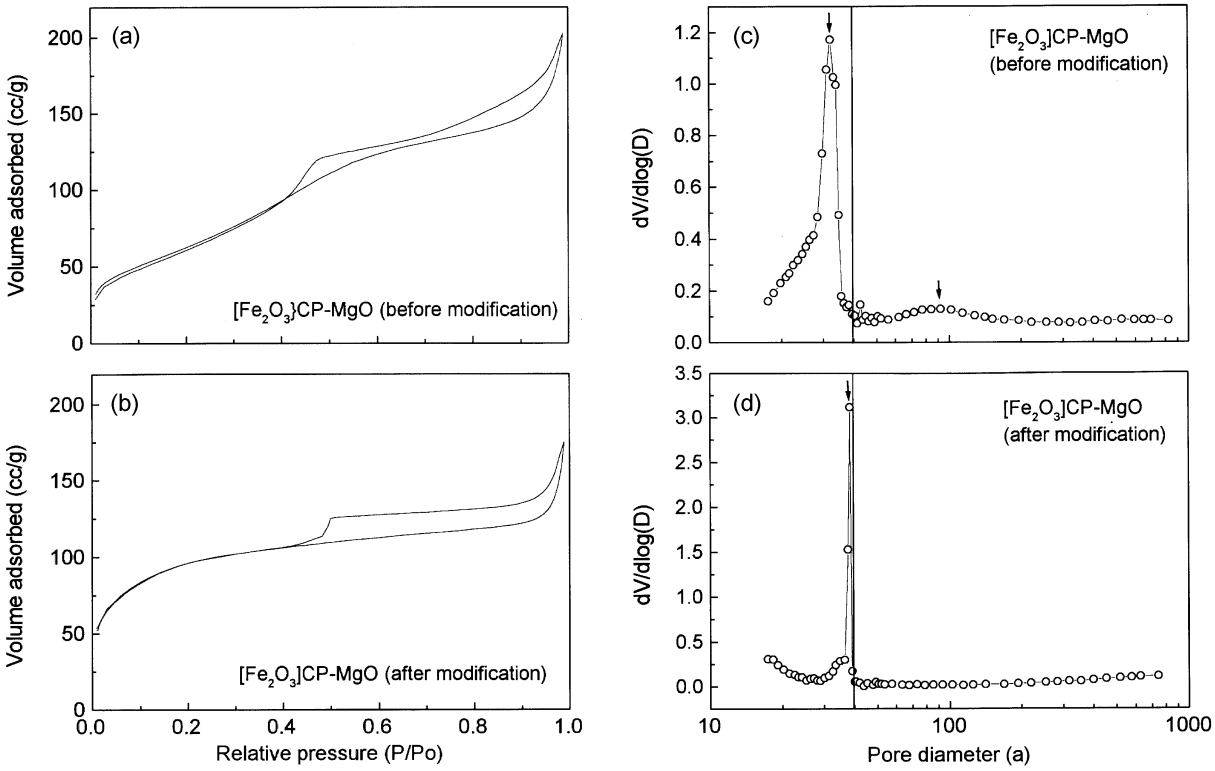

Figure 2. Isotherms of nitrogen adsorption-desorption on Fe_2O_3-coated CP-MgO, which is designated as [Fe_2O_3]CP-MgO. (a) before modification, and (b) after modification. Pore size distributions of [Fe_2O_3]CP-MgO, derived from those isotherms. (c) before modification, and (d) after modification. Pore characteristics of [Fe_2O_3]CP-MgO was modified by hydration in water-saturated air, followed by dehydration at 300 °C under dynamic vacuum.

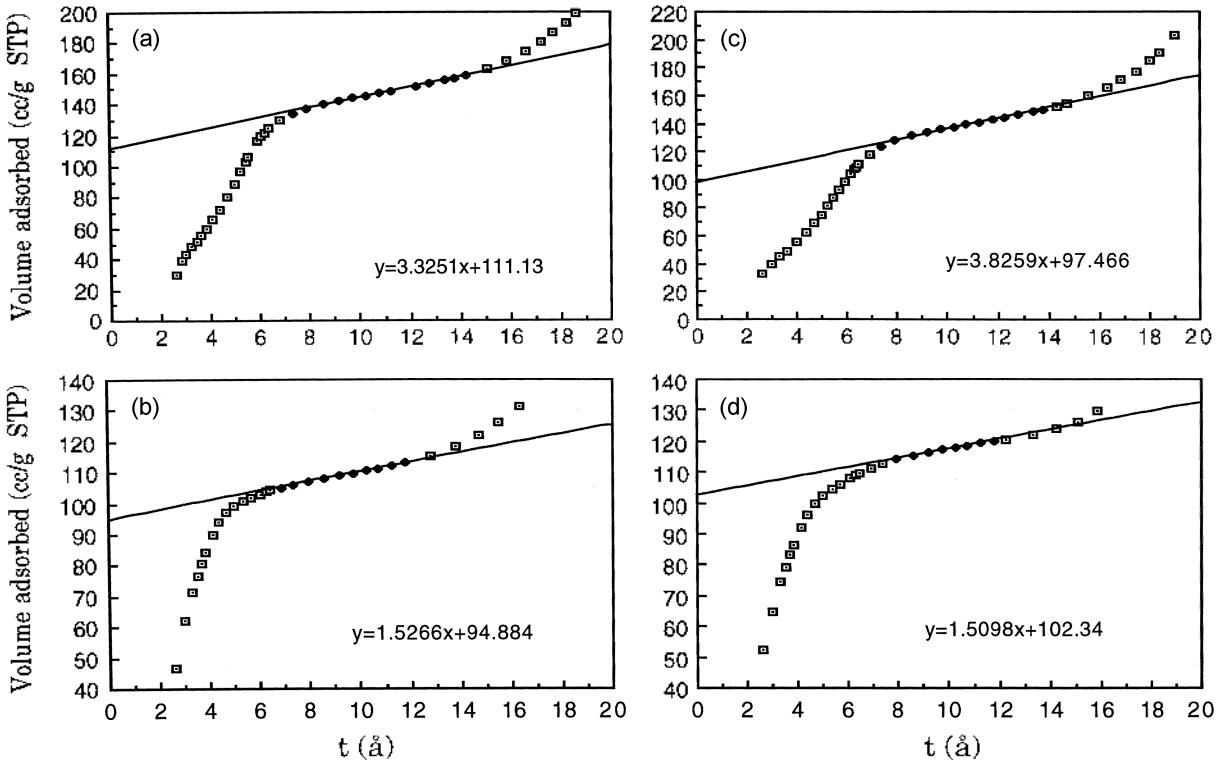

Figure 3. In order to calculate volume by micropores, t-plots were derived from the nitrogen adsorption-desorption isotherms, for (a) CP-MgO before modification, (b) CP-MgO after modification, (c) [Fe_2O_3]CP-MgO before modification, and (d) [Fe_2O_3]CP-MgO after modification.

Table 1. Pore characteristics of CM-MgO,[24] CP-MgO, and $[Fe_2O_3]$CP-MgO

	Before modification					After modification				
	S_{total}	S_{micro}	$\%S_{micro}$	V_{pore}	$r_{average}$	S_{total}	S_{micro}	$\%S_{micro}$	V_{pore}	$r_{average}$
CM-MgO	9.83 m^2/g	1.91 m^2/g	19.4%	0.0233 cc/g	94.87 Å	23.83 m^2/g	16.86 m^2/g	70.8%	0.0360 cc/g	60.38 Å
CP-MgO	271.01	219.80	81.1	0.3028	44.69	344.01	320.50	93.2	0.2370	27.56
$[Fe_2O_3]$CP-MgO	232.87	173.95	74.7	0.2949	50.66	348.59	325.34	93.3	0.2459	28.22

micropores. From fitted slope of the curves, surface area generated by the micropores was assessed and provided in Table 1. For the comparison, data on CM-MgO were recapped in first line of the table.[24] Compared to the CM-MgO, total surface area of CP-MgO is ~30 fold larger (<10 versus 270 m^2/g). The surface areas obtained from the t-plots indicate that more than 81% of the surface is from the micropores in the CP-MgO. On the contrary, CM-MgO has only 20% of its surface made out of micropores.[24] As pointed out in the experimentals section, a major difference in processing between CM-MgO and CP-MgO is extent of hydration.[24] PXRD patterns (Figure 4a and 4b) show that surface hydration proceeded deeply into the bulk, turning most of MgO into $Mg(OH)_2$. Surface area of the hydrated-MgO was only 28 m^2/g. Therefore, CP-MgO gained most of its surface area (from 28 to 270 m^2/g) during dehydration at 500 °C under dynamic vacuum. During thermal dehydration, phase transformation from $Mg(OH)_2$ to MgO occurred

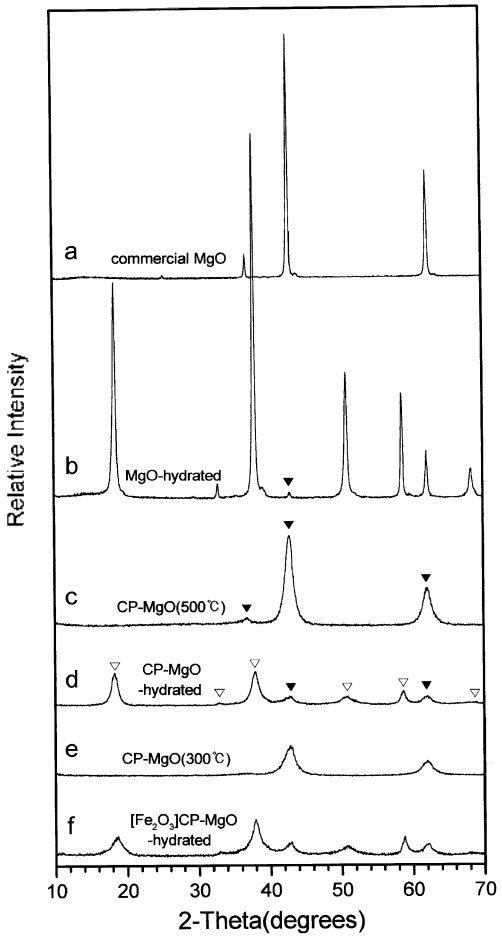

Figure 4. Powder X-ray diffraction patterns obtained during each step of the sample preparation. (a) Commercially purchased MgO as it is. (b) After deep hydration in boiling water. (c) After dehydration at 500 °C under dynamic vacuum, it turns into the broad pattern (nano-grains) by CP-MgO. (d) Upon rehydration, broad peaks of $Mg(OH)_2$ are apparent. (e) After dehydration at 300 °C under dynamic vacuum, it returns back to the broad pattern of the MgO. (f) Broad pattern of $Mg(OH)_2$ is obtained by hydration of $[Fe_2O_3]$CP-MgO. Open triangles designate peaks for $Mg(OH)_2$, and closed ones for MgO.

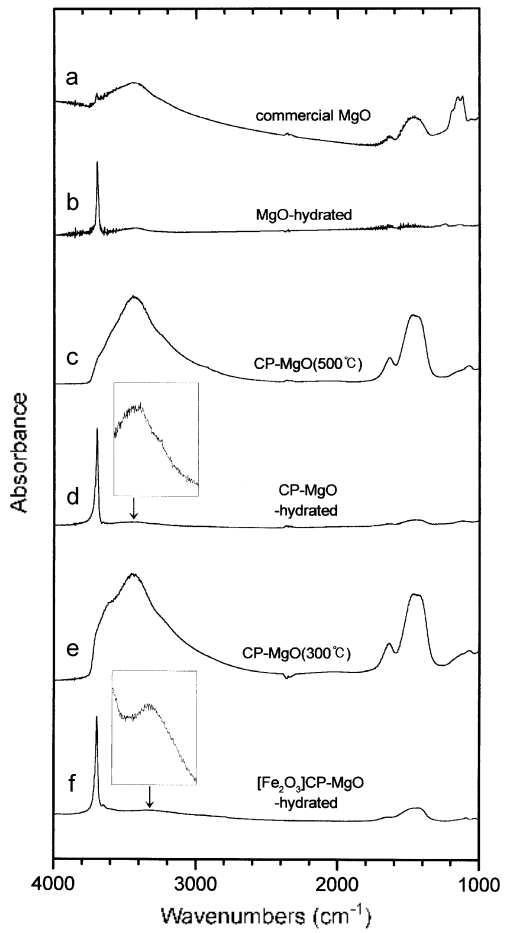

Figure 5. FTIR spectra obtained during each step of the sample preparation. (a) Commercially purchased MgO as it is (bulk). (b) After deep hydration in boiling water. (c) After dehydration at 500 °C under dynamic vacuum (nano-grains). (d) After hydration by water-saturated air. (e) After dehydration at 300 °C under dynamic vacuum, it returns back to the MgO. (f) After hydration (water-saturated air) of $[Fe_2O_3]$CP-MgO. The intensity is in an arbitrary unit.

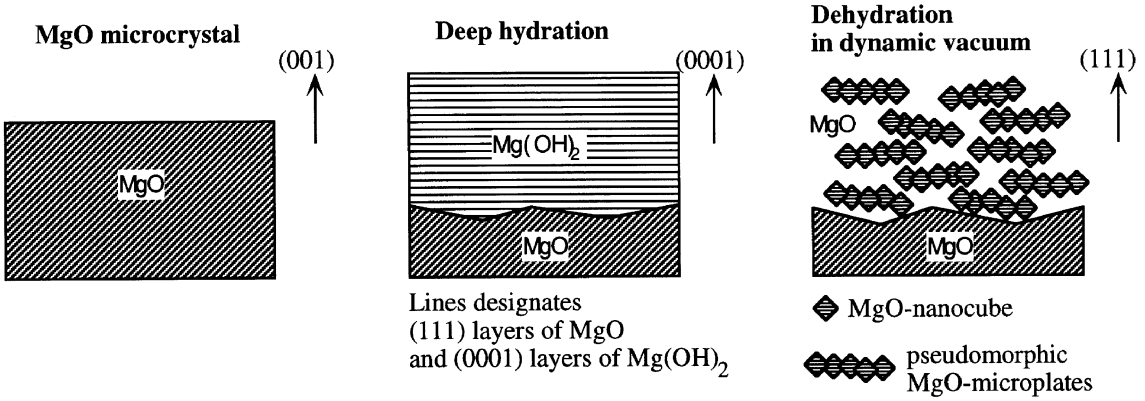

Scheme 1. Proposed mechanism of generation of CP-MgO, by deep hydration (in boiling water) of MgO, followed by dehydration at 500 °C under dynamic vacuum. This hypothetical scheme is proposed on the basis of previously known mechanisms of decomposition of brucite ($Mg(OH)_2$) into MgO, and of pore characterization in this report.

(Figure 4c), which apparently generated noticible amount of micropores (Table 1).

On the basis of known phenomena observed during thermal decomposition of brucite,[17-24] an explanation is proposed in Scheme 1 on how the porosity was generated. Upon being exposed to water, (100) surface of MgO is known to reconstruct into (111)-hydroxyl surface, which is topologically very close to (0001) facet of $Mg(OH)_2$.[9] As hydroxylation proceeds further into the bulk, topotactic transformation of (111)-hydroxyl to (0001) facet generates a layer of $Mg(OH)_2$ over MgO. As the frontline proceeds into the bulk, the layer of $Mg(OH)_2$ becomes thicker, which is manifested by PXRD pattern in Figure 4b, and FTIR spectrum in Figure 5b. PXRD pattern shows strong diffractions by $Mg(OH)_2$. A sharp IR peak at 3700 cm^{-1} is by isolated hydroxyls, and one around 3400 cm^{-1} is broadened by adsorbed water.[28,29] Upon being heated under dynamic vaccum, surface layer of $Mg(OH)_2$ decomposes into MgO. It is presumed that the decomposition follows the way others have reported on thermal decomposition of bulk brucite.[17-24] Pseudomorphic microplates of MgO would be generated from $Mg(OH)_2$. These microplates should be facing each other, generating slit type mesopores, as are menifested by the pore analysis in this study. Wedge-like shape of the slits indicates the relative position of those plates is not parallel. Somehow, relative positions of the plates are distorted and tilted. It is proposed that the microplates are composed of nano-grains (nanocubes) of MgO.[17,18,20] PXRD pattern of CP-MgO in Figure 4c shows very broad diffraction peak, which is typical for nanocrystalline MgO. Size of the crystallites, which is calculated by Sherrer's equation, is 6 nm. Because (0001) direction in $Mg(OH)_2$ corresponds to (111) direction in MgO, the corner of the nanocubes should be pointing perpendicular to the surface. As the corners of the cubes are pointing toward (111) direction, (100) facets of the adjacent cubes should be facing each other. Thereby, slit type micropores would be generated between those (100) facets of adjacent MgO nanocubes.

We happened to find that the shape of the pore was gradually changing when CP-MgO was remained in an ambient air. If CP-MgO was kept in a tightly closed container, such change was not observed. It is obvious that surface hydroxylation plays an important role in such change, by considering the change proceeds more readily in humid air.

By applying this finding, the pore of the CP-MgO was modified into a specific shape. The modification was carried out by hydrating CP-MgO into $Mg(OH)_2$ in water-saturated air, followed by dehydration at 300 °C under dynamic vacuum, transforming $Mg(OH)_2$ back into MgO. After the modification, the nitrogen isotherm shows an ideal shape of H3-type hysteresis (Figure 1b), indicating the bimodal mesopores have changed into unimodal ones. Abrupt release of adsorbed nitrogen at relative pressure of around 0.5 indicates the slit has parallel opening with specific dimension. Accordingly, pore size distribution curve has a sharp peak at specific dimension, shown at Figure 1d. The dimension of the slit is 32 Å for CP-MgO. Surface area obtained from t-plot shows the fraction of the micropores is further increased to 93% (Figure 3 and Table 1).

It is proposed that the extent of surface hydroxylation could influence the conformation of the porosity, as shown in Scheme 2. $Mg(OH)_2$ is known to transform completely into MgO at 300 °C.[22] But, studies by others showed that some surface hydroxyls adamantly remained still at the temperature.[29,30] In situ IR study showed that hydroxylated surface was still intact at 300 °C,[30] though the amount was decreased substantially at 500 °C. At 500 °C, MgO cubes and plates are suggested to be partially connected by condensation reaction among surface hydroxyls on them. It is early step toward sintering. Consequently, relative position of those cubes becomes distorted and tilted, generating wedge-shaped micropores. At the same time, adjacent plates approach each other *via* condensation reaction among surface hydroxyls, concomitantly widening the other side. Thereby, size distribution became bimodal, as was shown in the pore analysis. As the sample is exposed to high humidity, the condensation reaction is reversed. Unlike in the microcrystalline MgO, hydration of the CP-MgO proceeds readily

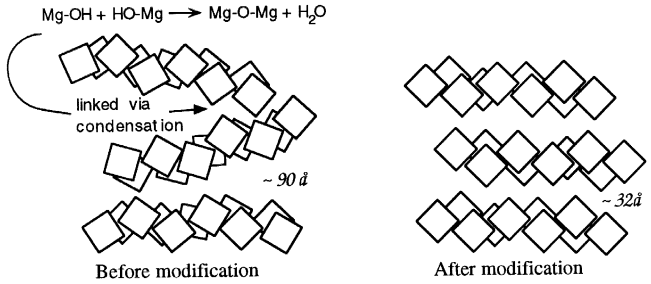

Scheme 2. Proposed mechanism of pore modification by hydration in water-saturated air, followed by dehydration at 300 °C under dynamic vacuum.

into the bulk (Figure 4d). It is suggested that hydrolysis reaction occurs preferentially at connected parts of the crystallites, where curvature is the highest.[31] As the crystallites (cubes and plates) are disconnected *via* rehydration, distorted position is straightened. As dehydration reaction was carried out at lower temperature, relative position of MgO facets stays parallel each other, which gives nitrogen isotherm in perfect H3 type. At the same time surface area by micropores increases (from 81 to 93%) as more wedges are opened up into parallel slits.

Interestingly, application of Fe_2O_3 over MgO didn't brought noticeable change in the feature of the isotherms (comparing Figure 1a, 1b, and Figure 2a, 2b). Apparently, the Fe_2O_3 on MgO also didn't change other pore characteristics such as pore shape, and pore volume. Only a minor variation was that the size distribution of the mesopores became narrower and shifted toward slightly larger size (compare Figure 1 and 2 over reference line). Because Fe was loaded *via* complex formation of molecular $Fe(acac)_3$ onto active sites on the surface of CP-MgO, the entire surface was suggested to be loaded with Fe_2O_3.[14,16,24] Corroborating to this suggestion, the amount of Fe loaded on the surface of $[Fe_2O_3]$CP-MgO is proportional to the surface area of MgO core, as is shown in Table 2. Apparently, the micropores of CP-MgO were not plugged up by applying Fe_2O_3, by seeing that 75% of surface area is still from micropores in $[Fe_2O_3]$CP-MgO (Figure 3 and Table 2). These observations indicate that the distribution of Fe_2O_3 is highly uniform over the entire surface of MgO.

With the Fe_2O_3 present over the MgO, hydration still proceeds deep into the bulk as in the CP-MgO, producing thick layer of $Mg(OH)_2$ (Figure 4f). Like in the CP-MgO, dehydration at 300 °C generates parallel slits with specific dimension. The dimension of the slit, 38 Å (Figure 2d), is larger than in the CP-MgO. Therefore, it appears that overall dimension of the pore is increased as Fe_2O_3 is applied over the MgO (see also the average radius in Table 1). FTIR spectra in Figure 5d and 5f show that the broad peak around 3450 cm^{-1} is shifted toward lower energy, indicating -OH on the surface became more acidic as Fe was present. Broadness of the peak is caused by hydrogen-bonding interaction with physisorbed water, which ascertains that it is from the species on the surface.[28,29] In this regard, it's worth to revisit Figure 1c and 1d. It is shown that a small population of macropores (~600 Å) is consistently and reproducibly observed in CP-MgO, but not in $[Fe_2O_3]$CP-MgO. In an ambient condition, -Mg-O- on the surface readily turns into Mg-OH by chemisorption of water, whereas -Fe-O- does not. It is speculated that particles of CP-MgO are anchored to each other through interaction among -Mg-OH groups on their surface, thereby generating large macropores.[24] On the contrary, the particles of $[Fe_2O_3]$CP-MgO apparently does not connect each other, indicating outer surface is composed mostly of Fe_2O_3. Therefore, Fe_2O_3 appears to be remained on the surface during and after the cycle of hydration-dehydration. These observations strongly suggest that 'spill-over' reaction has occurred during the modification process. Similar phenomenon has also been observed in the previous study on nano-beads of AP-MgO and $[Fe_2O_3]$AP-MgO.[15,16]

It was reported that more SO_2 physisorbs on CP-MgO than on AP-MgO at high partial pressure,[15] even though surface area of the CP-MgO is much smaller than that of the AP-MgO (270 versus 370 m^2/g). By considering the pore characteristics of CP-MgO is strikingly different from those of AP-MgO, it is speculated that this seemingly contradicting observation was caused by different shape and composition of the pores. AP-MgO has both necked and cylindrical pores.[16] Having more surface area, AP-MgO may adsorb more chemical than CP-MgO at low partial pressure. But, at high partial pressure, where capillary force starts to act, it is suggested that slit-shaped pores of CP-MgO can accommodate more chemical condense than conical pores of AP-MgO.

Table 2. Fe contents for samples of Fe_2O_3-coated MgO, with different BET-surface areas

surface area (m^2/g)	Fe loading (w%)
37	0.15
241	0.88
325	1.43

Conclusions

Surface area of MgO was greatly increased by thermally decomposing hydrated sample at 500 °C under dynamic vacuum. Drastic increase (around 100-fold) of the surface area, from several m^2/g to 270 m^2/g, was caused mostly by generation of micropores during thermal dehydration. More than 80% of total surface area was from micropores. Mesopores had wedge-like shape with bimodal size distribution.

The pore characteristics were further modified by going through hydration in water-saturated air, followed by subsequent dehydration at 300 °C. The wedge-like mesopores were changed into parallel slits with very specific dimension of 32 Å. Surface area was further increased to 340 m^2/g, and most of it (93%) was by micropores.

These observations suggest that MgO-porosity is closely related to generation of MgO nanocubes, and isomorphic MgO microplates. The space between the cubes constitutes

slit shaped pores. Considering the isomorphism, the shape of the micropores is also suggested to be similar to that of the mesopores. It appears that partial sintering made the space formed into a wedge, which was later relieved back into parallel slit by surface hydration.

Application of Fe_2O_3 over CP-MgO does not brought noticeable change in the pore characteristics, other than slight expansion of pore dimension. During phase transformation between MgO and $Mg(OH)_2$, Fe_2O_3 was remained on the surface possibly *via* 'spill-over'. Therefore, modification of pore characteristics could be carried out without restriction of whether outer layer of Fe_2O_3 was present or not.

Acknowledgement. This research was supported by the Sookmyung Women's University Research Grants 2000, and by KOSEF through R06-2002-007-01005. Provision of nitrogen adsorption-desorption isotherms by Dr. S. S. Nam is acknowledged with a gratitude.

References

1. Gillan, M. J.; Kantorovich, L. N.; Lindan, P. J. D. *Current Opinion in Solid State & Materials Science* **1996**, *1*, 820.
2. Causa, M.; Dovesi, R.; Pisani, C.; Roetti, C. *Surface Science* **1986**, *175*, 551.
3. Scamehorn, C. A.; Hess, A. C.; McCarthy, M. I. *J. Chem. Phys.* **1993**, *99*, 2786.
4. Scamehorn, C. A.; Harrison, N. M.; McCarthy, M. I. *J. Chem. Phys.* **1994**, *101*, 1547.
5. Pugh, S.; Gillan, M. J. *Surface Science* **1994**, *320*, 331.
6. Langel, W. L.; Parrinello, M. *J. Chem. Phys.* **1995**, *103*, 3240.
7. Kantorovich, L. N.; Holender, J. M.; Gillan, M. J. *Surface Science* **1995**, *343*, 221.
8. Nada, R.; Hess, A. C.; Pisani, C. *Surface Science* **1995**, *336*, 353.
9. Refson, K.; Wogelius, R. A.; Frager, D. G.; Payne, M. C.; Lee, M. H.; Milman, V. *Phys. Review B* **1995**, *52*(15), 52.
10. Lin, S.-T.; Klabunde, K. J. *Langmuir* **1985**, *1*, 600.
11. Li, Y.-X.; Klabunde, K. J. *Langmuir* **1991**, *7*, 1388.
12. Li, Y.-X.; Koper, O.; Atteya, M.; Klabunde, K. J. *Chem. Mater.* **1992**, *4*, 323.
13. Klabunde, K. J.; Khaleel, A.; Park, D. *High Temp. Mater. Sci.* **1995**, *33*, 99.
14. Stark, J. V.; Park, D. G.; Lagadic, I.; Klabunde, K. J. *Chem. Mater.* **1996**, *8*, 1904.
15. Klabunde, K. J.; Stark, J.; Koper, O.; Mohs, C.; Park, D. G.; Decker, S.; Jiang, Y.; Lagadic, I.; Zhang, D. *J. Phys. Chem.* **1996**, *100*, 12142.
16. Kim, H. J.; Kang, J.; Park, D. G.; Kweon, H.-J.; Klabunde, K. J. *Bull. Korean Chem. Soc.* **1997**, *18*, 831.
17. Green, J. *J. Mater. Sci.* **1983**, *18*, 637.
18. Moodie, A. F.; Warble, C. E. *J. Crystal Growth* **1986**, *74*, 89.
19. Beruto, D.; Botter, R. *J. Am. Ceram. Soc.* **1987**, *70*(3), 155.
20. Kim, M. G.; Dahmen, U.; Searey, A. W. *J. Am. Ceram. Soc.* **1987**, *70*(3), 146.
21. Carrott, M. R.; Carrott, P.; Brotas de Carvalho, M. *Characterization of Porous Solids II*; Rodriguez-Reinoso, F. *et al.*, Eds; Elsevier: Amsterdam, 1991; p 635.
22. Carrott, M. R.; Carrott, P.; Brotas de Carvalho, M.; Sing, K. S. W. *J. Chem. Soc. Faraday Trans.* **1991**, *87*(1), 185.
23. Goodman, J. F. *Proc. R. Soc. London Ser. A* **1958**, *247*, 346.
24. Kim, H.-J.; Kang J.; Song, M. Y.; Park, S. H.; Park, D. G.; Kweon, H.-J.; Nam, S. S. *Bull. Korean Chem. Soc.* **1999**, *20*(7), 786.
25. Lowell, S.; Shield, J. E. *Powder Surface Area and Porosity*, 3rd Ed.; Chapman & Hall: London, UK, 1991; p 11.
26. Johnson, M. F. L. *J. Crystal.* **1978**, *52*, 425.
27. Gregg, S. J.; Sing, K. S. W. *Adsorption, Surface Area and Porosity*, 2nd Ed.; Academic press: London, UK, 1982; p 111.
28. Carrott, M. R.; Carrott, P.; Brotas de Carvalho, M.; Sing, K. S. W. *J. Chem. Soc. Faraday Trans.* **1993**, *89*(3), 579.
29. Anderson, P. J.; Horlock, R. F.; Oliver, J. F. *Trans. Faraday Soc.* **1962**, *58*, 1993.
30. Coluccia, S.; Marchese, L.; Lavagnino, S.; Anpo, M. *Spectrochimica Acta* **1987**, *43A*(12), 1573.
31. Brinker, C. J.; Scherer, G. W. *Sol-Gel Science The Physics and Chemistry of Sol-Gel Processing*; Academic press: San Diego, US, 1990; p 360.